Engineering Structures 301 (2024) 117276

Contents lists available at ScienceDirect

Engineering Structures

journal homepage: www.elsevier.com/locate/engstruct

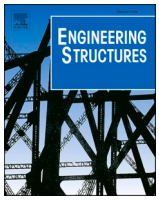

Explainable machine learning model for predicting punching shear strength of FRC flat slabs

Tongxu Liu [a], Celal Cakiroglu [b], Kamrul Islam [c], Zhen Wang [d], Moncef L. Nehdi [e,*]

[a] Department of Civil, Geological and Mining Engineering, Polytechnique Montréal, Canada
[b] Department of Civil Engineering, Turkish-German University, 34820 Istanbul, Turkey
[c] Department of Civil, Geological and Mining Engineering, Polytechnique Montréal, Canada
[d] Key Laboratory of Concrete and Prestressed Concrete Structures of Ministry of Education, School of Civil Engineering, Southeast University, Nanjing 211189, PR China
[e] Department of Civil Engineering, McMaster University, Hamilton, ON L8S 4L8, Canada

ARTICLE INFO

Keywords:
Slab-column joint
Punching shear strength
Fiber reinforced concrete
High performance concrete
Ultra high-performance concrete, Machine learning
XGBoost, SHAP analysis

ABSTRACT

Reinforced concrete slabs are vulnerable to punching shear failure at the slab-column joint, which can initiate catastrophic progressive collapse. The addition of steel fibers in the concrete matrix has emerged as an effective strategy to mitigate such progressive failure. However, the effects of the diverse mixture proportions of the concrete matrix with different types and dosages of fibers have made the accurate prediction of the punching shear strength (PSS) of the fiber-reinforced concrete (FRC) flat slabs a complex task, where the existing mechanical models have several limitations. Therefore, this study proposes an explainable XGBoost model for predicting PSS of flat slabs made with different types of FRC based on a newly established comprehensive database of 251 flat slabs including normal strength FRC slabs, high-performance FRC slabs, and ultra-high-performance FRC slabs. A customized procedure was proposed to establish the XGBoost model considering data preparation, feature selection, hyperparameter tuning and model validation. The performance of the XGBoost model was then compared with that of existing mechanical models. Finally, sensitivity analysis and SHapley Additive exPlanations (SHAP) analysis were applied to identify the most influential parameters on the prediction of PSS. Results show that the proposed feature selection method is effective in identifying six influential parameters from the eleven parameters related to the PSS of FRC flat slabs. The developed XGBoost model yielded highest prediction accuracy and lowest variation, which outperformed the other mechanical models. Sensitivity analysis also indicated similar trends of parameters in both the XGBoost model and the mechanical models. The PSS of FRC flat slabs can be improved by increasing the concrete compressive strength, reinforcement ratio, and fiber volume, and by decreasing the column width-to-depth ratio, water-to-binder ratio, and aggregate size ratio. The proposed XGBoost model could enhance the understanding of PSS of FRC flat slabs and guide future pertinent design code provisions.

1. Introduction

Reinforced concrete (RC) flat slabs are commonly used in structural systems owing to their ease of construction and architectural advantages. However, these structural members are prone to punching shear failure due to their small effective shear resisting area [1,2]. The punching shear failure of RC flat slabs can lead to a progressive collapse of the entire structure as observed in recent decades [3–5]. Research showed that the load-carrying capacity of RC flat slabs is usually determined by the punching shear strength (PSS) near the slab-column connections, where using stirrups is usually not practical due to the shallow depth of the slab [6,7]. In such connections, significant load drop can be observed before the yielding of the longitudinal bars, and a cone-shaped shear failure in the circular zone surrounding the column can occur without warning. To improve the punching shear behavior of concrete slabs, various studies have investigated the beneficial effects of using steel fibers at the connections or in the entire concrete slabs [8–11]. Fibers can not only bridge shear cracks and control crack propagation, but also increase the shear strength, toughness, and post-peak behavior of concrete [12,13]. Using fiber reinforced concrete

* Corresponding author.
E-mail addresses: tongxu.liu@polymtl.ca (T. Liu), cakirogl@ualberta.ca (C. Cakiroglu), kamrul.islam@polymtl.ca (K. Islam), sdkj199017@163.com (Z. Wang), nehdim@mcmaster.ca (M.L. Nehdi).

https://doi.org/10.1016/j.engstruct.2023.117276
Received 23 February 2023; Received in revised form 20 November 2023; Accepted 30 November 2023
Available online 8 December 2023

(FRC) has thus proven to be a viable way to improve the punching shear capacity and ductility of slab-column connections [14–17]. Moreover, high-strength steel fibers coupled with high-performance cementitious matrices can further increase the strength and crack resistance of concrete [18]. This leads to superior mechanical properties of higher fiber-matrix bond strength, higher tensile strength, and extended tensile strain hardening behavior in the high-performance FRC (HPFRC) and ultra-high-performance FRC (UHPFRC) compared with the normal strength FRC (NSFRC). Therefore, enhanced punching shear behavior of slab-column connections can be expected in the HPFRC and UHPFRC flat slabs [19–22].

However, the diverse proportions of concrete matrix and types of fibers in the NSFRC, HPFRC, and UHPFRC have caused a great challenge in accurately predicting the associated punching shear strength of the flat slabs using these materials. Several prediction models for conventional concrete slabs proposed in several standards such as ACI 318–19, BS-8110–97, and Eurocode 2 [23–25] may be inadequate for NSFRC, HPFRC, and UHPFRC slabs since they neglect the contribution of steel fibers to shear strength [26]. There are some prediction models intended for slabs made by NSFRC where parameters like the fiber volume, fiber length, and fiber diameter are included. These models consider the fiber contribution mainly through two methods. The first is via regression analysis, whereby the coefficients of parameters related to fibers are fitted using experimental data for a group of NSFRC slabs [15,27,28]. This method is usually restrained by the limited number of data points used. The second method is the fiber-matrix bond mechanism, which adopts the fiber-matrix bond strength from fiber pullout and other material properties tests [6,29]. However, because of fiber orientation, fiber type, and concrete matrix composition, high variability can be found in the fiber bond strength [30], which also limits the accuracy of the prediction model [31]. In addition, these models do not consider HPFRC and UHPFRC slabs, where the fiber-bond strength and corresponding fiber contribution vary as a function of the fiber content, water-to-cement ratio, aggregate size, and other pertinent parameters related to the concrete mixture composition [32,33]. Therefore, new robust and comprehensive models are required for predicting the punching shear strength of FRC slabs.

The application of data-driven machine learning (ML) algorithms has become increasingly popular in the last few years owing to the enhanced prediction capability of newly developed algorithms [34,35]. ML models can allow the creation of generative design and learn from big data with very low computational cost. They are first trained using a known dataset and then used to predict the responses of an unknown dataset, which makes them a robust prediction tool in various challenging engineering problems [36,37]. Researchers have successfully implemented ML models to predict the material properties of concrete and the structural capacity of concrete structures [38–42].

For the specific case of punching shear strength of concrete slabs, there are already several ML models tailored for conventional RC slabs [43–46], and for RC slabs strengthened with FRP bars [47,48]. Among these, XGBoost was found to be an effective model with superior accuracy [45,46]. Conversely, there is a dearth of research on ML models for FRC slabs. Hoang [49] demonstrated the application of a sequential piecewise linear regression (SPMLR) model and artificial neural networks (ANN) to the problem of the PSS prediction of FRC slabs, where six parameters and 140 data samples were considered. Lu *et al.* [50] used the same database of 140 samples and 6 parameters via several tree-based ML models. A feature selection method was considered to improve the model prediction accuracy. Alotaibi *et al.* [51] developed neuro-nomographs using the results of an ANN-based algorithm considering 8 parameters. The prediction agreed well with the 148 datasets of FRC slabs. Although substantial knowledge can be obtained through ML techniques, these predictive models cannot be directly applied to the slabs using HPFRC and UHPFRC where the fiber size, content and orientation, and properties of the cementitious matrix deviate significantly from conventional NSFRC and introduce uncertainty. Moreover, the Blackbox nature of such models does not allow the user to interpret the prediction or explain the trends. Therefore, there is a need to develop explainable ML algorithms and establish predictive models for the punching shear strength that are more intuitive and interpretable to help the practical engineering design of FRC flat slabs.

Accordingly, the objective of this study is to develop and implement an explainable predictive XGBoost model for the prediction of the PSS of flat slabs using different types of FRC. A comprehensive database comprising 251 flat slabs including NSFRC, HPFRC, and UHPFRC slabs was first established from an extensive search of the open literature. Based on the database, a predictive model based on the XGBoost algorithm was trained by a customized procedure including data preparation, feature selection, hyperparameter tuning and model validation. To evaluate the predictive performance of the XGBoost models with and without feature selection, its predictions were compared with that of another three ML models widely used in concrete structures, three mechanical models from the structural standards (only for normal strength concrete slabs), and three mechanical models from existing research (for NSFRC slabs). The SHAP algorithm and sensitivity analysis was subsequently applied to analyze the prediction model and to quantify the contribution of different input variables to the PSS and explain the complex input-output relationship of the developed ML model, as opposed to the black-box nature of existing models. It is shown that the predictive model could lead to a better understanding of the punching shear behavior of FRC flat slabs and assist in rational and accurate predictions of the punching shear capacity in engineering practice.

2. Overview of selected machine learning models

2.1. XGBoost algorithm

The XGBoost algorithm was used to establish the proposed model owing to its well-established superior performance in various prediction applications for the behavior of concrete structures [46,52,53]. The prediction function of the XGBoost model can be expressed as shown in Eq. 1, which requires providing a dataset of $((X_1,y_1),(X_2,y_2),\ldots,(X_i,y_i),\ldots,(X_n,y_n))$ that adopts the typical boosting procedure, starting from the initial weak learner to constitute the final strongest learner. $f^{XGB}(X)$ is the sum of m decision trees $T_M(X)$, and the M^{th} decision tree is optimized according to the residual value of the prediction based on the previous (M - 1) trees and corresponding test value. A detailed description of the algorithm can be found in Chen *et al.* [54] and Feng *et al.* [52].

$$f^{XGB}(X)=\sum_{m=1}^{M}T_m(X)=f_{M-1}(X)+r_{M-1}=f_{M-1}(X)+\alpha T_M(X) \tag{1}$$

To evaluate the performance of XGBoost models, several widely used algorithms, such as support vector regression (SVR), K-nearest neighbors (KNN), and random forest regression (RFR) were adopted aiming at the development of corresponding models for comparison with XGBoost models.

2.2. SVR algorithm

The SVR model mainly uses mapping functions to transform the data into a higher-dimensional space, where the linear separation can be determined by maximizing the margin between different classes [55,56]. The function of the SVR model can be presented as shown in Eq. 2, where the feature space X is matrix of features ($x_1,x_2,\ldots,x_n$) and n is the number of features. $f(X)$ is the prediction of target variable by the algorithm which is determined by the feature space X, the normal vector $\boldsymbol{w}$ and intercept b [57]. φ is the mapping function which transformed the features into a higher-dimensional space.

$$f^{SVR}(X) = \boldsymbol{w}\varphi(X) + b \tag{2}$$

2.3. KNN algorithm

The KNN model is a non-parametric model which cannot be described by a fixed number of parameters. It predicts the target variable by averaging the test values of the K known data points (y_k, $k = 1, 2, \ldots, K$), which refers to the nearest neighbors [58]. The K is the number of neighbors which are selected by evaluating the distance between a data point to other points through the Euclidean distance metric in the data space [59]. The prediction can be obtained as shown in Eq. 3:

$$f^{KNN}(X) = \sum_{k=1}^{K} y_k \tag{3}$$

2.4. RFR algorithm

The RFR model extends the bagging algorithm to obtain high accuracy and limit the degree of overfitting [40,60]. Each decision tree is determined by randomly selecting a subset of features and a subset of samples from the database [61]. The final prediction is achieved by averaging the prediction values of numerous decision trees. The function of RFR model can be presented in Eq. 4, where $T_m(X)$ is the prediction of the m^{th} tree, and M is the number of decision trees.

$$f^{RFR}(X) = \frac{1}{M}\sum_{m=1}^{M} T_m(X) \tag{4}$$

3. Database establishment for flat slabs with different types of FRC

3.1. Data collection

The comprehensive database of experimental tests conducted to measure the PSS of FRC slabs v_p was established based on the data of 251 test specimens retrieved from pertinent studies in the open literature. That data was processed and classified by the standard cylinder compressive strength $f_c^{'}$, which yielded 135 FRC slabs ($f_c^{'} \leq 60$ MPa), 33 HPFRC slabs ($60 \leq f_c^{'} \leq 120$ MPa), 26 UHPFRC slabs ($f_c^{'} \geq 120$ MPa), along with 57 conventional RC slabs (made of concrete with no fibers, and used as reference slabs). The data was retrieved from 30 peer-reviewed studies published by diverse research groups [9,11–15,17,20,62–81]. All the collected test results reported punching shear failure of the tested specimens and no flexural failure. The PSS v_p is calculated by the punching shear capacity V_p obtained from tests divided by the effective depth d and critical perimeter $b_0 = 4(c+d)$ [23], which is $v_p = V_p/b_0 d$. A summary of the constructed database is provided in the Table 1. A total of 11 input parameters were included in the database to construct the ML models for predicting the target variable of PSS v_p, which were selected according to the following steps.

Firstly, eight parameters were selected from the studies of previous databases which have non-negligible effects on the prediction of punching shear strength of RC and NSFRC slabs [20,43–45,49,50,51,82,83]. They mainly include the effective depth of the slab d, column width c (if the column is circular, it is converted to an equivalent square column by considering the same critical shear perimeter [45]), shear span a, standard cylinder compressive strength of concrete $f_c^{'}$, tensile

Table 1
Summary of the FRC slabs database.

Reference	Year	Test No.	Concrete Type	w/b	f_c (MPa)	d_g (mm)	V_f (%)	Fiber type*	ρ (%)	f_y (MPa)	v_p (MPa)
Swamy and Ali[13]	1982	10	FRC	0.47	36.8–41.1	10	0–1.2	1, 2, 3	0.56–0.75	462	1.98–2.81
Narayanan and Darwish[28]	1987	12	FRC	0.4–0.55	29.8–53.0	0.6	0–1.25	2	1.6–2.53	550	3.15–4.68
Theodorakopoulos and Swamy[11]	1993	15	FRC	0.4	14.2–38.0	6–20	0–1	2, 3, 6, 7	0.37–0.56	460	1.37–2.71
Shaaban and Gesund[12]	1994	12	FRC	0.4	22.1–46.7	40	0–1.93	5	1.55	400	2.38–4.47
Tan and Paramasivam[62]	1994	14	FRC	0.3–0.5	37.6–60.6	10	0.31–2	3	0.35–1.05	560	1.25–2.85
Harajli *et al.*[15]	1995	8	FRC	0.4	24.6–31.8	10	0–2	3	1.49–1.59	501	2.69–3.94
McHarg *et al.*[63]	2000	4	FRC	0.5	30.0–41.5	20	0–0.5	3	1.11–2.15	434	2.10–3.01
Harris 2004[64]	2004	7	UHPFRC	0.12	221.3	0.6	2	1	0	-	4.68–5.89
Park and Hong[65]	2005	6	UHPFRC	0.23	120.9–126.6	0.6	0.5–1.5	1	0	-	3.50–6.09
Ozden *et al.*[66]	2006	10	FRC, HPFRC	0.4	19.3–81.3	20	0–1	3	0.73–2.26	471–507	1.57–5.76
Yaseen[67]	2006	14	FRC, HPFRC	0.28–0.5	35.4–65.1	9.5	0–1	1	1.61	670	3.53–5.56
Naaman *et al.*[68]	2007	2	HPFRC	0.35–0.5	44.9–69.6	0.6–10	0–1	8	0.49–0.65	414	2.70–8.21
Hanai and Holanda[69]	2008	9	FRC	0.34–0.65	23.1–59.7	6.3	0–2	3	1.51	400	2.68–4.61
Joh *et al.*[70]	2008	2	UHPFRC	0.2	194	0.6	2	1	0	-	5.42–6.51
Wang *et al.*[71]	2009	5	FRC	0.4	14.9–20.2	20	0–1.5	1	0.98	400	2.13–2.63
Cheng and Parra-Montesinos [17]	2010	10	FRC	0.4–0.49	25.4–59.3	13	0–1.5	3, 8	0.66–0.98	449–471	2.67–3.74
Yang *et al.*[72]	2010	2	FRC	0.4	30.8–35.3	20	0–0.5	3	1.34	666	1.85–1.95
Higashiyama *et al.*[27]	2011	12	FRC	0.53–0.57	21.6–42.4	20	0.63–1.03	3	0.40–0.91	377	1.63–3.34
Nguyen-Minh *et al.*[9]	2012	12	FRC	0.4	21.7–25.3	22	0–0.76	3	0.83	492	2.22–3.10
Hassan[73]	2012	20	HPFRC	0.144–0.45	37.5–118	0.6–5	0–2	3	0.32–0.74	395–435	2.77–10.28
Grimaldi *et al.*[74]	2013	4	FRC	0.4	48.4–50.8	20	0–0.5	3	1.05	520	2.51–3.65
AlQuraishi[75]	2014	7	UHPFRC	0.175–0.61	40.3–208.3	0.6–16	0–1.1	1	1–2.01	562–570	2.99–6.86
Caratelli *et al.*[76]	2016	2	FRC	0.35–0.36	42.2–46.8	4–16	0–0.38	3	1.05	520	2.61–4.0
Nguyen *et al.*[20]	2017	7	HPFRC	0.21	86.8–99.0	0.6	0–1.6	1	2.83	400	5.79–11.20
Gouveia *et al.*[77]	2017	5	FRC	0.45	45.4–55.7	12.8	0–1.5	3	0.76–1.5	529–534	3.80–7.77
Chanthabouala *et al.*[14]	2018	10	HPFRC	0.4	80.0–100.0	20	0–1.2	4	0.92–1.47	575–585	2.57–6.82
Abdel-Rahman *et al.*[78]	2018	10	FRC	0.54	24	20	0–1.5	5	1.19	400	1.69–2.46
Landler and Fischer[79]	2019	8	FRC	0.4	39.8–48.9	20	0–1	4	1.23	523	2.83–4.20
Kadhum *et al.*[80]	2020	4	UHPFRC	0.18–0.35	38.4–130.2	0.6–4.75	0–2	1	0.67	535	4.28–8.59
Shoukry *et al.*[81]	2020	8	UHPFRC	0.17–0.45	47.2–127	0.6–20	0–3	3, 5	1.76	400	3.99–7.61

*Type of fibers: 1 for straight fibers, 2 for crimped fibers, 3 for hooked fibers, 4 for 4D/5D hooked fibers, 5 for corrugated fibers, 6 for paddle fibers, 7 for Japanese fibers, 8 for Twisted fibers

reinforcement ratio ρ (calculated by the sectional area of a single rebar A_s divided by the effective depth d and rebar spacing s, that is $\rho = A_s/sd$), yield strength of tensile reinforcement f_y, fiber volume V_f, and fiber aspect ratio a_f (calculated by fiber length l_f divided by fiber diameter, that is $a_f = l_f/d_f$). The critical parameter b_0 mentioned in the existing mechanical models is not considered because it can be considered by the combination of c and d in the ML models.

Secondly, in order to consider the special characteristics of the HPFRC and UHPFRC slabs, four new parameters in the database were added the database in this study based on the experimental and theoretical studies of these slabs: (i) For the concrete properties, two additional parameters, namely the maximum aggregate size d_g and water-to-binder ratio w/b, were included to differentiate the cementitious matrices of FRC, HPFRC, and UHPFRC, especially UHPFRC which is often made with very low w/b and elimination of coarse aggregates; (ii) For the fiber addition, another parameter fiber called fiber bond factor b_f was considered via the fiber types as suggested in mechanical models [6], with 0.4 for straight fibers, 0.6 for crimped, corrugated, and paddle fibers, and 0.8 for hooked fibers. For 4D/5D hooked fibers and twisted fibers, higher bond behavior was reported in the literature, and thus the bond factor can be 1.0 [14–18]; (iii) Some studies investigated using FRC or UHPFRC only in part of the slab. This was represented in this study by introducing a new parameter called fiber distribution ratio r_f, which is calculated by the distribution length L_f along shear span a (fibers were applied in this region) divided by shear span a. The illustration of the selected parameters is depicted in Fig. 1.

Thirdly, to eliminate the size effect, parameters with dimensions (d, c, a, d_g) are transferred to dimensionless parameters including column width-to-depth ratio c/d, shear span-to-depth ratio a/d and aggregate size ratio d_g/d_{g0} (calculated by maximum aggregate size d_g divided by the reference aggregate size d_{g0} in concrete). The d_{g0} is equal to 16 mm as suggested by Muttoni [1]. The value distributions of the parameters in terms of the target variable v_p were shown in Fig. 2. Compared with the existing database on the PSS of NSFRC, this new database has wider ranges in most of the parameters, especially the compressive strength of concrete, water/cement ratio, aggregate size ratio, and fiber volume, which is mainly due to additional consideration on the HPFRC and UHPFRC slabs. The ratio of the number of data points (251) and features (11) is 22.8, which lies in the range of ratios in recent studies related to machine learning models of concrete structures [41,46,56,57,84,85]. Fig. 2 also indicated that no clear and explicit relationship was found between any input parameter and the target variable. The non-linearity effect of the parameters may contribute to the difficulty of constructing an explicit mechanical model. Therefore, ML models can be considered as a viable alternative to the existing models to reach superior prediction accuracy.

4. Development of machine learning model

The development of the XGBoost model consists of three main steps: data preprocessing, feature selection, and hyperparameter tuning. These procedures can be conducted using the widely used python package scikit-learn [86] as illustrated in Fig. 3. After the development, the final optimized ML models were validated by predicting the PSS in the test set of the database. The model can be treated as acceptable if the results of the prediction performance in the test set are higher or at least not obviously lower than the average prediction performance of the cross-validation sets. The validation results are shown in Section 5. Besides, the other ML models (SVR model, RFR model, and KNN model) were also developed through a similar procedure for comparison.

4.1. Data preprocessing

First, feature scaling was conducted to normalize the data of each parameter into the range of [0,1] using the Min-Max scaler in scikit-learn [86]. Second, the 251 data points were divided into a training set of 201 data points (80% of the database) and a test set of 50 data points (20% of the database), as suggested by previous research [56,57,87]. Third, the typical 10-fold cross-validation technique was also used in the training set to help optimize the developed ML model [52], as shown in Fig. 3.

4.2. Feature selection

A feature selection procedure previously proposed by the authors can be conducted, which has been proved to eliminate redundant features without affecting the prediction performance of the ML models [41,57]. Firstly, features were ranked by combined weighted values (CWVs), as shown in Fig. 4. The CWV is the average of four values obtained from four methods of evaluating the relative importance of different features and is confirmed to be more stable than using a single feature selection method [41]. It should be noted that the water-to-binder ratio w/b achieved the highest CWV, which is mainly due to the newly collected database which aimed at distinguishing the difference between various fiber reinforced concretes. Besides the w/b, another two parameters to distinguish fiber-reinforced concrete include the concrete compressive

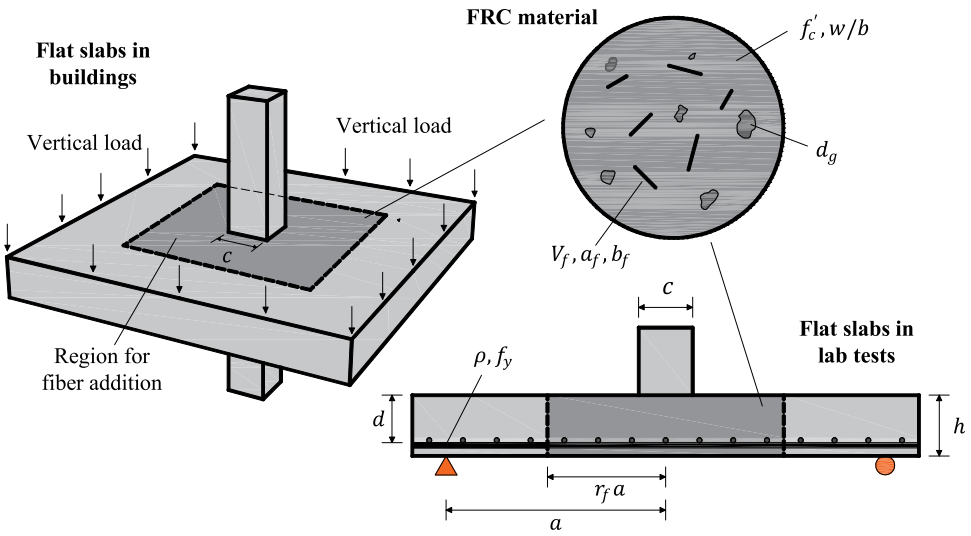

Fig. 1. Illustration of collected parameters for the database of punching shear strength of FRC slabs.

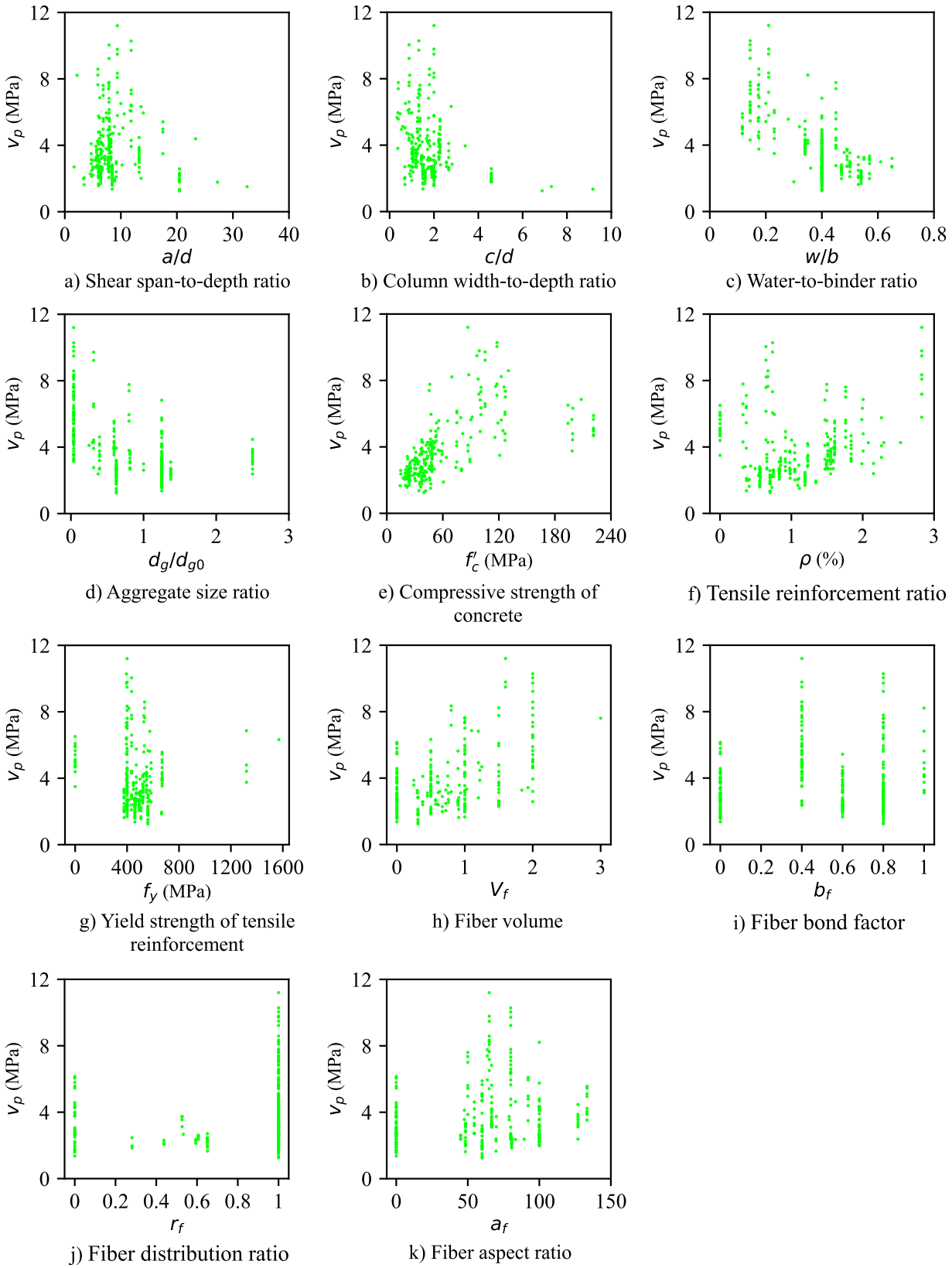

Fig. 2. The value distributions of the selected 11 parameters.

strength $f_c^{'}$ and aggregate size ratio d_g/d_{g0} also reach high CWVs. Secondly, the improved recursive feature elimination with the cross-validation (improved RFECV) method was used to determine the number of features used for developing final ML models [41]. The method progressively optimizes models with different number of features. In this study, 11 models were optimized in each ML algorithm by going through the data processing (including the 10-fold cross-validation) and hyperparameter tuning described in the previous

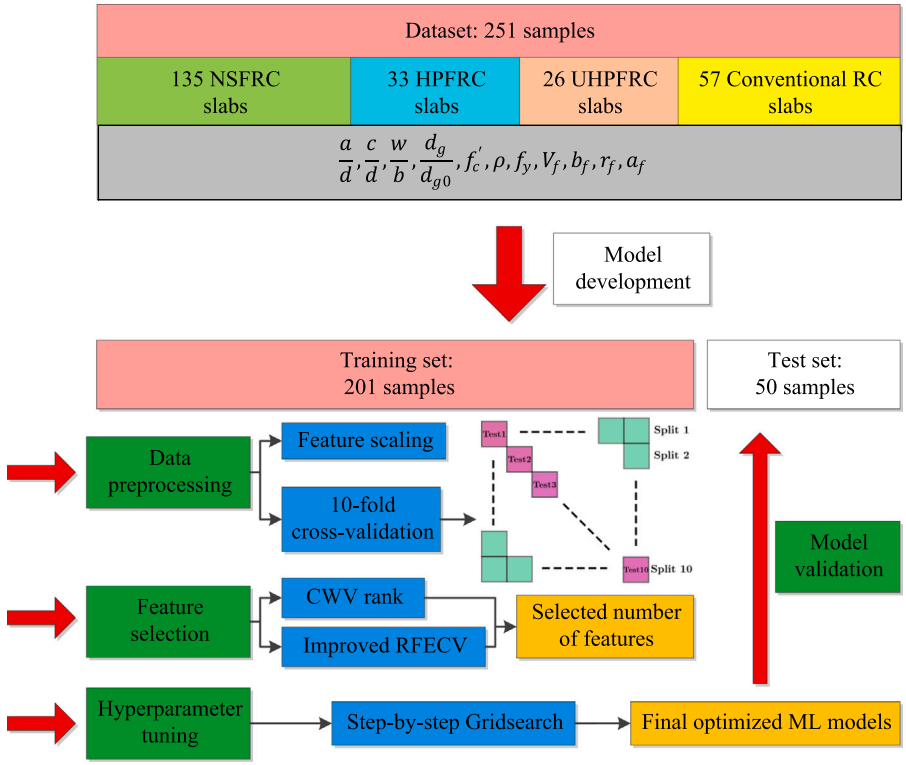

Fig. 3. Procedure for establishing ML models.

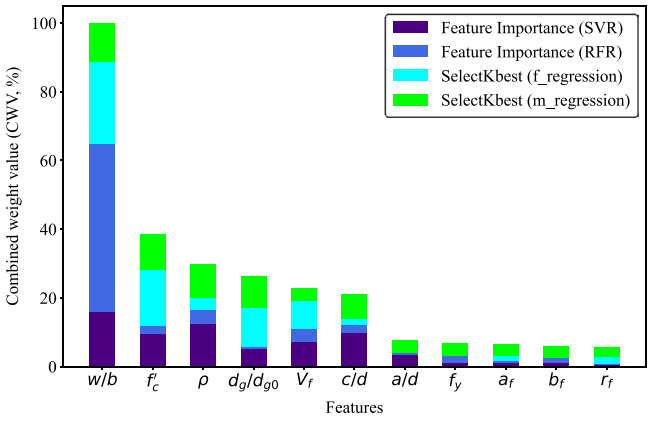

Fig. 4. CWV rank of all features in descending order.

and the next Sections (4.1 and 4.3). The initial model contains all 11 features, and each subsequent model eliminates the feature with the smallest CWV value until reaching the last model, which only includes one feature with the highest CWV value. The root-mean-squared error (RMSE) value was used as the scoring method, where m represents the number of samples, and y_i and y_{pi} represent the tests value and predicted value of the PSS of the i th sample. For each model, RMSE values of the 10 cross-validation sets were shown via boxplot. The boxplots with different numbers of features were shown in Fig. 5a-d for the four selected ML models. Fig. 5 showed that generally when the number of features included is small, the mean RMSE value of the 10 cross-validation sets was obviously decreased with the increase of the number of features, while the decrease is very limited when the number of features included is high. In each subfigure, the number of features used for developing final ML models was determined when the further increase in the number of features yielded no noticeable improvement in the prediction accuracy of the punching shear strength. As shown in Fig. 5, all four ML models selected 6 features as an acceptable performance (marked by red arrow) of the RMSE values. Each of the feature can lead to smaller value or less variation of RMSE, thus improving the prediction performance, while the other 5 features can be eliminated from the database due to their negligible effects on the target variable. It is interesting to note that the span-to-effective depth ratio a/d, which proved to have considerable influence on the punching shear capacity V in the existing literature [51,85,88,89] is not included in the selected features. This may be due to two reasons: First, this study selected the punching shear strength v_p as the target variable, which already considered the effect of the effective depth d. Second, the span length a itself was found to have very limited effects on the punching shear capacity [51]. Therefore, the elimination of the parameter a/d is considered as reliable.

$$RMSE = \sqrt{\frac{1}{m}\sum_{i=1}^{m}\left(y_i - y_{pi}\right)^2} \tag{5}$$

4.3. Hyperparameter tuning

The selected four ML algorithms all have three or more hyperparameters to determine, indicating that the typical one-step Gridsearch method would be very time-consuming. Thus, the sequential step-by-step Gridsearch, as suggested by Wang *et al.* [75], was adopted in the current study. The RMSE was used as the scoring method in the optimization procedures. At first, default values were used for all the hyperparameters. In each step, only two parameters were chosen to create a parameter grid for searching, while other parameters remain the same. The procedure ends when all the parameters are selected more than once, and the results tend to be stable. The meaning of the hyperparameters, the sequence of the optimization procedure, and the final value of the hyperparameters of the four ML models are shown in Table 2. It should be noted that in the XGBoost model, several regularization hyperparameters are considered including γ_{xgb}, α, λ, while other models use no or only one regularization hyperparameter. The

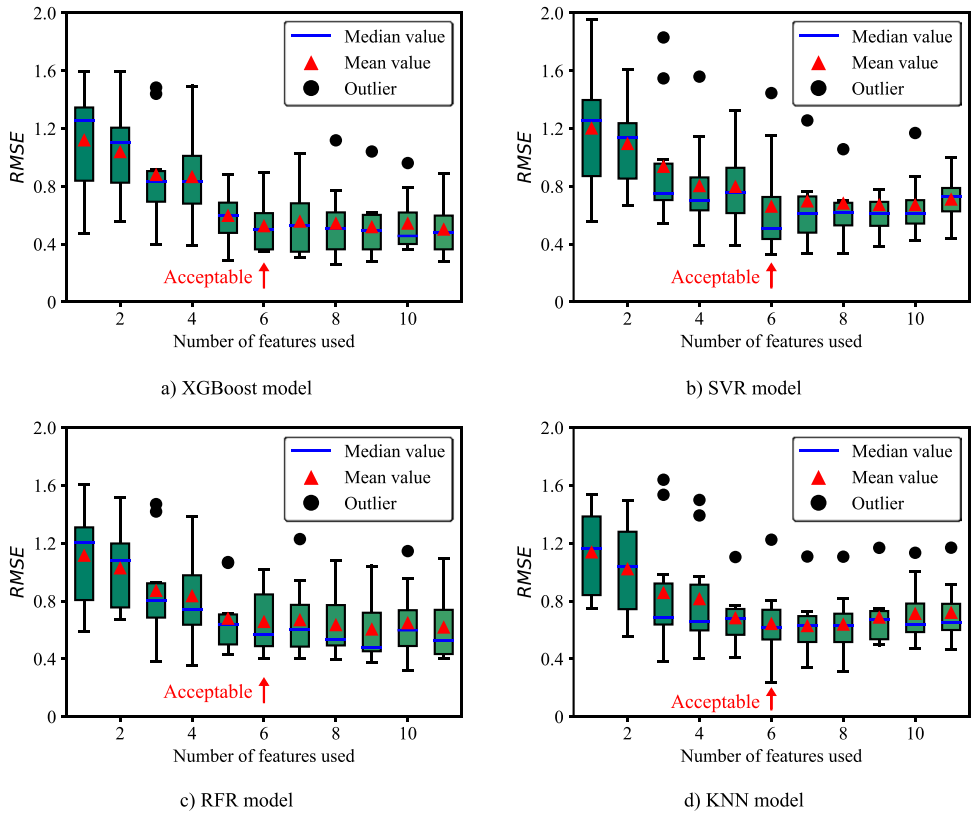

Fig. 5. Boxplots of RMSE values with different numbers of features in the ML models.

overfitting of these models can be evaluated in the next section.

5. XGBoost model evaluation

5.1. Comparison with other machine learning models

The four ML models are evaluated using six performance indicators that are adopted in the performance evaluation of data-driven ML models dealing with concrete structures. These include the mean value (MV), coefficient of variation (COV), guarantee rates for 100% and 125% of test values (GR100, GR125), mean absolute error (MAE), and coefficient of determination (R^2) [38,54,55]. The equations of these performance indicators are shown in Eqs. 6 to 10. The results of the ML models with feature selection are presented in Fig. 6. A model with a higher R^2 and lower error values indicates the best predictive data-driven model.

$$MV = \frac{1}{m}\sum_{i=1}^{m}\frac{y_{pi}}{y_i} \tag{6}$$

$$COV = \frac{1}{\frac{1}{m}\sum_{i=1}^{m}\frac{y_{pi}}{y_i}}\sqrt{\frac{1}{m-1}\sum_{i=1}^{m}\left(\frac{y_{pi}}{y_i}-\frac{1}{m}\sum_{i=1}^{m}\frac{y_{pi}}{y_i}\right)^2} \tag{7}$$

$$GR100 = P\left(\frac{y_{pi}}{y_i} \le 100\%\right) \tag{8}$$

$$\mathrm{GR125} = P\left(\frac{y_{pi}}{y_i} \le 125\%\right) \tag{9}$$

$$MAE = \frac{1}{m}\sum_{i=1}^{m}\left|y_i - y_{pi}\right| \tag{10}$$

$$R^2 = 1 - \frac{\sum_{i=1}^{m}\left(y_i - y_{pi}\right)^2}{\sum_{i=1}^{m}\left(y_i - \frac{1}{m}\sum_{i=1}^{m}y_i\right)^2} \tag{11}$$

Fig. 6 indicates that the XGBoost model performed the best among the four models, exhibiting lower COV and RMSE values, higher guarantee rates and R^2 values, and more stable MV values than the other three ML models in both cross-validation (CV) sets and test set. The superior accuracy of the XGBoost model stems from its boosting algorithm, where the residue value can be progressively decreased by ensembling the series of weak models. The RFR model attained the second-best accuracy, which may be due to it ensembling methods. The KNN model recorded the largest MAE and lowest R^2 values in the three types of data sets, which is due to its simple technique that was unable to eliminate outliers in the database. Although there is slight variance in prediction performance between the training set and CV sets due to the step-by-step Gridsearch tuning method, the difference is limited and is thus acceptable between the CV sets and test set, which proved that the model could lead to predictable results with limited variance for the unknown input data. The XGBoost model also performed better than the other machine learning models in reducing the variance between CV sets and test set. The results demonstrate the effectiveness of the XGBoost model in predicting the punching shear strength of FRC slabs. Accordingly, the XGBoost model was selected for further analysis.

5.2. Comparison with existing mechanical models

Six mechanical models were selected for predicting the PSS of FRC slabs. Three models are from standard provisions developed for conventional NSC slabs, since there were no models for FRC slabs in existing provisions, the models for NSC slabs were used for comparison to see their abilities to predict the PSS of FRC slabs. The other three specifically

Table 2
Hyperparameters for all optimized ML models.

Model	Selected hyperparameters	Optimization procedure	Final chosen hyperparameters
SVR	ϵ: *Epsilon in the epsilon-SVR model* C: Regularization parameter γ_{svr}: Gaussian kernel coefficient	(ϵ, C) – (γ_{svr}, C)	$\epsilon = 0.037$ $C = 50.71$ $\gamma = 6.07$
KNN	n_n: Number of neighbors to use p: Power parameter for the Minkowski metric w: Weight function used	(p, n_n) – (p, w)	$n_n = 3$ $p = 1.0$ w = *'distance'*
RFR	n_t: Number of trees in the forest f_{max}: Number of features considered in searching the best split s_{ob}: Whether to use out-of-bag samples to estimate the generalization score d_{max}: Maximum depth of the tree s_{min}: Minimum number of samples required to split an internal code l_{min}: Minimum number of samples required to be at a leaf node	(n_e, f_{max}) – (s_{ob}, d_{max}) – (s_{min}, l_{min}) – (n_e, d_{max})	$n_e = 40$ $f_{max} = 3$ s_{ob} = 'False' $d_{max} = 8$ $s_{min} = 2$ $l_{min} = 1$
XGBoost	l_r: Boosting learning rate n_g: Number of gradient boosted tree d_{max}: Maximum depth of the tree w_{min}: Minimum sum of instance weight needed in a child γ_{xgb}: Minimum loss reduction required in partition on a leaf node w_{scale}: Parameter balancing of positive and negative weights s_{sub}: Subsample ratio of the training instance s_{tree}: Subsample ratio of columns when constructing each tree α: L1 regularization term on weights λ: L2 regularization term on weights	(l_r, n_g) – (d_{max}, w_{min}) – (γ_{xgb}, w_{scale}) – (s_{sub}, s_{tree}) – (α, λ) – (l_r, n_g)	$l_r = 0.10$ $n_e = 180$ $d_{max} = 12$ $w_{min} = 2$ $\gamma_{xgb} = 0.05$ $w_{scale} = 0.2$ $s_{sub} = 0.7$ $s_{tree} = 0.7$ $\alpha = 0.4$ $\lambda = 0.8$

target NSFRC slabs from existing literature [15,27,28]. The equations for the six mechanical models are presented in Eqs. 12–17. In Eq. 12 and Eq. 16, β represents the ratio of the longer dimension to the shorter dimension of the column section, which always equals 1 in this study. The results of the six models were compared with that of the XGBoost model (Table 3) by the six performance indicators presented in Section 5.1. It can be observed that the XGBoost models outperformed the mechanical models, achieving 1.01 in MV, 0.07 in COV, 0.17 in MAE, 98.8% in GR125, and 0.99 for R^2.

ACI 318–19 [23].

$$v_p = \min\left[\frac{1}{3}, \frac{1}{6}\left(1+\frac{2}{\beta}\right), \frac{1}{12}\left(2+\frac{\alpha_s d}{4c+4d}\right)\right]\lambda_s\sqrt{f_c'} \tag{12a}$$

$$\lambda_s = \sqrt{\frac{2}{1+0.004d}} \le 1 \tag{12b}$$

$$\alpha_s = 40 \tag{12c}$$

BS-8110–97 [24].

$$v_p = 0.79\sqrt[4]{\frac{400}{d}}\sqrt[3]{\frac{100\rho f_{cu}}{25}}\frac{c+3d}{c+d} \tag{13a}$$

$$f_{cu} = f_c'/0.8 \tag{13b}$$

Eurocode 2 [25].

$$v_p = \frac{c+\pi d}{c+d}\max\left[0.18k\left(100\rho f_c'\right)^{\frac{1}{3}}, 0.035k^{\frac{3}{2}}\sqrt{f_c'}\right] \tag{14a}$$

$$k = \left(1+\sqrt{\frac{200}{d}}\right) \le 2 \tag{14b}$$

Narayanan and Darwish [28].

$$v_p = \frac{c+0.75\pi h}{c+d}\lambda_s\left(0.24f_{spf}+16\rho+v_b\right)(1-0.55F) \tag{15a}$$

$$f_{spf} = \frac{f_{cu}}{20-\sqrt{F}}+0.7+\sqrt{F} \tag{15b}$$

$$\lambda_s = 1.6-0.002h \tag{15c}$$

$$v_b = 1.7F \tag{15d}$$

$$F = V_f b_f a_f \tag{15e}$$

Harajli *et al.* [15].

$$v_p = \left(\min\left[\frac{1}{3}, \frac{1}{6}\left(1+\frac{2}{\beta}\right), \frac{1}{12}\left(2+\frac{\alpha_s d}{4c+4d}\right)\right]+0.096V_f\right)\sqrt{f_c'} \tag{16}$$

Higashiyama *et al.* [27].

$$v_p = \beta_d\beta_p\beta_r\left(f_{pcd}+v_b\right)(1-0.32F) \tag{17a}$$

$$f_{pcd} = 0.2\sqrt{f_c'} \le 1.2MPa \tag{17b}$$

$$\beta_d = \sqrt[4]{\frac{1000}{d}} \le 1.5 \tag{17c}$$

$$\beta_p = \sqrt[3]{100\rho} \le 1.5 \tag{17d}$$

$$\beta_r = 1+\frac{1}{1+0.25c/d} \tag{17e}$$

$$F = V_f b_f a_f \tag{17 f}$$

The predicted values are presented in the *y*-axis of Fig. 7 with respect to the corresponding actual experimental values in the x-axis for each model. The MV values are also indicated, along with the guarantee rates of GR100 and GR125, which are shown with the line of 100% and 125% to illustrate the accuracy and how conservative each model is. As indicated, the XGBoost models attained the highest level of accuracy and yielded the smallest prediction variation among all the investigated models. For the guarantee rates, the ACI 318–19 and Eurocode 2 models reached higher GR100, while the XGBoost models and ACI 318–19 model obtained higher GR125 values. The reason that the XGBoost model has prediction values higher than the test values in over 50% of the data points is that unlike the design code equations, no reduction factor is used. Nevertheless, the high GR125 values was reach in XGBoost model, which indicated that the prediction of the XGBoost model can become adequately conservative if a reduction factor of 0.8 is used.

Furthermore, to appraise the overall performance of the XGBoost models and mechanical models, the error distributions of each model are illustrated in Fig. 8. The percentage of error (calculated as predicted value subtracting the test value and then dividing by the test value) is

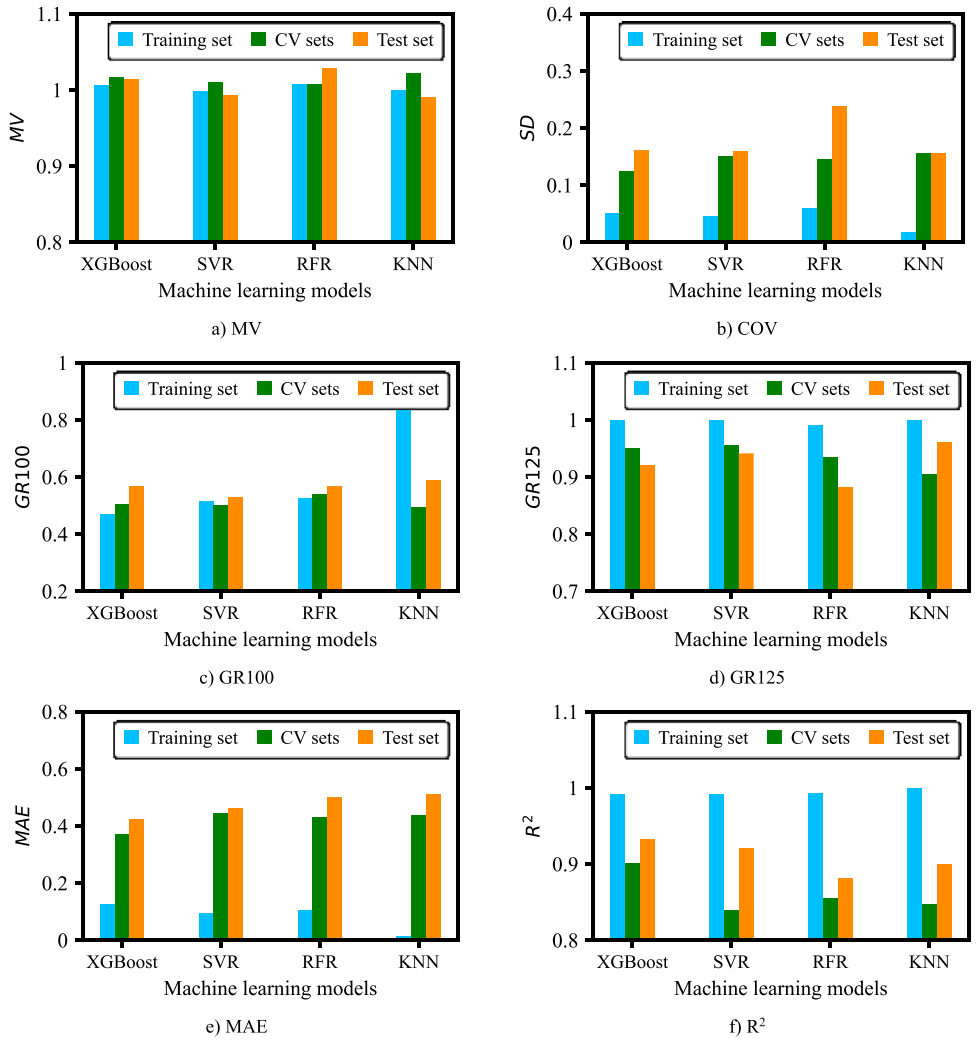

Fig. 6. Comparison of performance indicators in different ML models.

Table 3
Results of performance indicators for mechanical models and ML models.

	MV	COV	GR100 (%)	GR125 (%)	MAE	R^2
ACI 318–19	0.70	0.30	89.2	98.4	1.47	-4.58
BS-8110–97	0.81	0.39	77.7	94.0	1.26	-1.72
Eurocode 2	0.72	0.28	91.2	99.6	1.42	-6.17
Narayanan and Darwish	1.04	0.33	52.6	75.3	1.10	0.06
Harajli et al.	0.85	0.29	76.9	92.4	1.11	-0.22
Higashiyama et al.	1.12	0.42	34.3	57.8	1.51	-1.38
XGBoost	1.01	0.07	50.2	98.8	0.17	0.99

shown in terms of the percentage of predicted points (calculated as the number of points that is lower than the corresponding percentage of error divided by the total number of points). Accordingly, if the curve is closer to the model prediction as indicated by the dashed line, the corresponding model performs better on the prediction of the target variable (PSS). As indicated in Fig. 8, the two XGBoost models achieved similar high accuracy and low variance with errors distributed mostly in the range of (−25%, 25%). In contrast, the other mechanical-based models exhibited a much wider distribution of the percentage of error, leading to a substantial deviation in some data points.

6. Explanation of ML models using SHAP analysis

The SHapley Additive exPlanations (SHAP) algorithm has been applied as an effective method of explaining the input-output relationships of complex ML models in recent years. This algorithm quantifies the effects of different input parameters on the model output by assigning to each input parameter a SHAP value. These SHAP values are represented with ϕ_j in Eq. (18) [90]. The SHAP technique utilizes simplified models to explain the differences between the outputs of a model when an input feature is included and withheld from a model. These simplified models are denoted with $s(x')$ in Eq. (18) where $x' \in \{0,1\}$.

$$s(x') = \phi_0 + \sum_{j=1}^{M} \phi_j x_j' \tag{18a}$$

$$\phi_j = \sum_{S \subseteq F \setminus \{j\}} \frac{|S|!(|F|-|S|-1)!}{|F|!} \left[f_{S\cup\{j\}}\left(x_{S\cup\{j\}}\right) - f_S(x_S) \right] \tag{18b}$$

In Eq. (18), M denotes the total number of input parameters, F denotes the set of all input features and S is a subset of F which does not contain the input feature with the index j. In Eq. (18b), x_S is a vector which contains the values of the input parameters in the subset S. The SHAP values ϕ_j describes the impact of adding the feature with index j on the model predictions, the extent of impact of the value of each

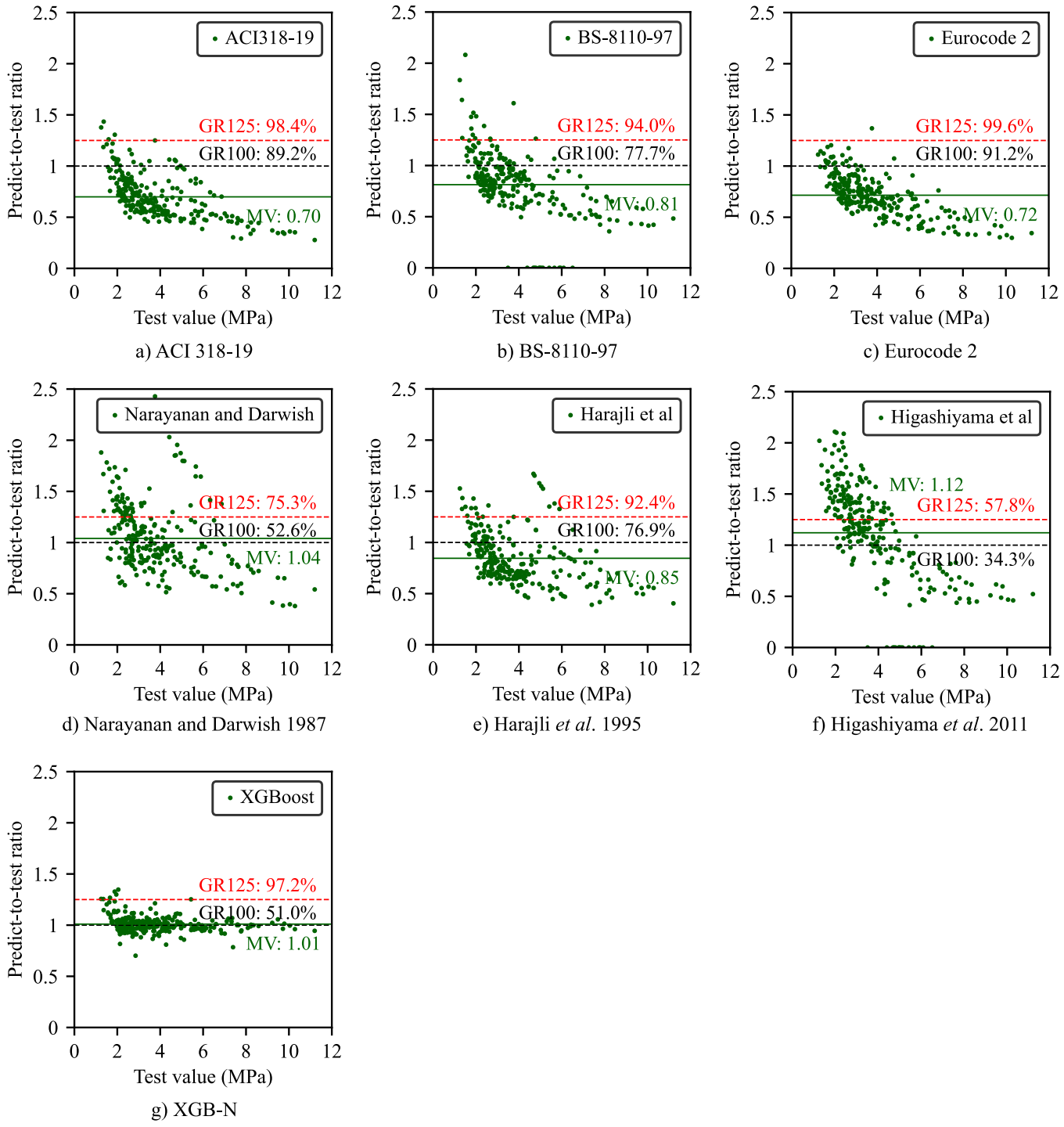

Fig. 7. Comparison of predicted-to-experimental value ratio for mechanical versus XGBoost models.

feature on the model output (target variable PSS) is quantified directly by SHAP values compared the base value of the feature, and the summation of the SHAP values of all the features included is the model output,.

This section presents the outcome of the SHAP algorithm for the predictive XGBoost model for interpretation. The SHAP summary plot shown in Fig. 9 is an information rich visualization of how different input parameters affect the PSS. The magnitudes of the parameters are indicated with color bars on the right side of each plot. Every data sample is represented in these plots with a dot. The positions of these dots in the horizontal direction convey information about the impact of a particular variable on the model prediction, namely SHAP values. Dots with high magnitude SHAP values correspond to high impact on the model output, whereas parameters with low impact are represented with dots clustered around a zero SHAP value or are positioned near the zero SHAP value. The distribution of dots in the vertical indicates that the numbers of points in the near area is large so that some of the dots shift vertically for clear presentation. For example, the concrete compressive strength$f_c^{'}$, the low values of $f_c^{'}$ lead to high negative SHAP values and the high values of $f_c^{'}$ lead to high positive SHAP values, which indicates a significant influence on the model output. However, for the longitudinal rebar ratio ρ, the low values of ρ lead to high or low

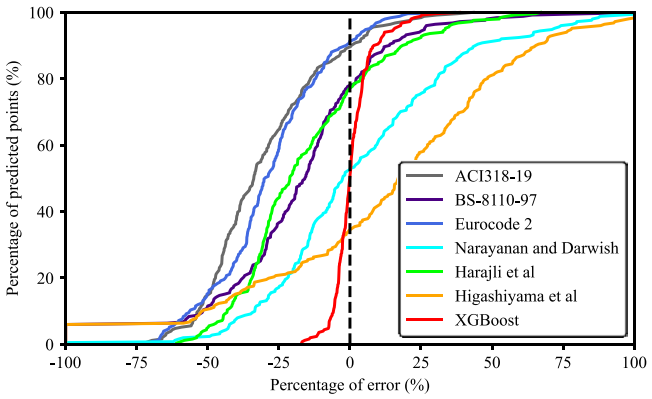

Fig. 8. Error distributions of mechanical models and XGBoost models.

negative SHAP value, while most of the high values of ρ lead to low positive SHAP value, so the longitudinal rebar ratio has relatively limited influence on the model output compared with the $f_c^{'}$.

Fig. 9 indicates that the compressive strength of concrete $f_c^{'}$, water-to-binder ratio w/b, steel fiber volume V_f, and longitudinal rebar ratio ρ are the variables with the most significant influence on the model prediction based on the SHAP algorithm. General trend of the parameters` influences on the target variable can be found that increasing the w/b, d_g/d_{g0}, or c/d has a decreasing effect on the target variable v_p, while the opposite trend is true for $f_c^{'}$, V_f and ρ.

To augment the summary plots and clarify certain relationships between the design variables, feature dependence plots have been generated in Fig. 10. Each one of the plots in Fig. 10 describes the variation of the SHAP value of the target variable with respect to the values of a specific parameter. Therefore, the six detailed relationships between the target variable and each parameter were obtained.

According to Fig. 10, increasing the values of $f_c^{'}$ are associated with higher SHAP values up to around 75 MPa, beyond this threshold value, the relationship between $f_c^{'}$ and its corresponding SHAP values becomes irregular. A similar relationship can be observed for V_f where increasing the values of the fiber volume leads to obviously higher SHAP values, until it reaches about 1.5%. Relatively consistent increase of the SHAP values due to the increase of longitudinal rebar ratio was found in the analysis until the ratio reached the 3%, indicating the effectiveness of longitudinal rebars even when the rebar ratio is high.

Contrary to the increasing effect of $f_c^{'}$, V_f and ρ, the other three parameters c/d, w/b, d_g/d_{g0} inversely affected the corresponding SHAP values, which means higher SHAP values are achieved by decreasing the values of these parameters. The decreasing effects of the three parameters are usually more significant when the parameter value is low, then become less substantial or insignificant after a certain threshold has been reached. For c/d, the threshold is about 4.5, while for w/b, d_g/d_{g0}, the threshold values are about 0.4, and 0.7, respectively.

The effects of the four parameters (c/d, $f_c^{'}$, V_f, ρ) agree well with the common knowledge on PSS of concrete slabs, while the effects of the other two parameters (w/b and d_g/d_{g0}) agree well with the knowledge on the FRC and UHPC tension members [91,92]. It is worth mentioning that the higher PSS of UHPFRC slabs, which is confirmed by the experimental results, can be proven in the SHAP dependence plots because that UHPFRC has lower water-to-binder ratio (w/b), low aggregate size ratio (d_g/d_{g0}) higher compressive strength ($f_c^{'}$) and higher fiber volume (V_f), which all contribute to higher SHAP values compared with NSFRC slabs, and thus contribute to a higher PSS.

7. Sensitivity analysis

The sensitivity analysis is the method to determine the changes of the target variable with respect to changes in the input parameters [93]. The objective of the analysis based on the proposed XGBoost model includes two aspects. Firstly, the detailed parameter trend (effects on the target variable from low to high values of a parameter) was compared with the existing mechanical models on FRC slabs, namely the Narayanan and Darwish in Eq. 15, Harajli *et al.* in Eq. 16 and Higashiyama *et al.* in Eq. 17, to discuss their agreement and differences. Secondly, the threshold of the parameters in which the further increasing of the parameter`s value cannot have obvious influence on the target value can be quantitatively determined. Four parameters including the concrete compressive strength $f_c^{'}$, reinforcement ratio ρ, fiber volume V_f, and perimeter-to-effective depth ratio c/d were selected in the analysis because they are also explicitly considered by the mechanical models. An ideal FRC slab was determined as the base slab by choosing the average values of the parameters in all the FRC slabs in the database (c/d = 1.74, w/b = 0.37, d_g/d_{g0} = 0.80, $f_c^{'}$ = 61.3 MPa, ρ = 1.10%, f_y = 469 MPa, V_f = 0.78%) [94,95]. When studying the effect of a parameter, only this parameter varies at the value range in the database (indicated in Fig. 2), while the other parameters are maintained constant similar to the base slab. The effects of the four parameters in the XGBoost model and the other three mechanical models are shown in Fig. 11.

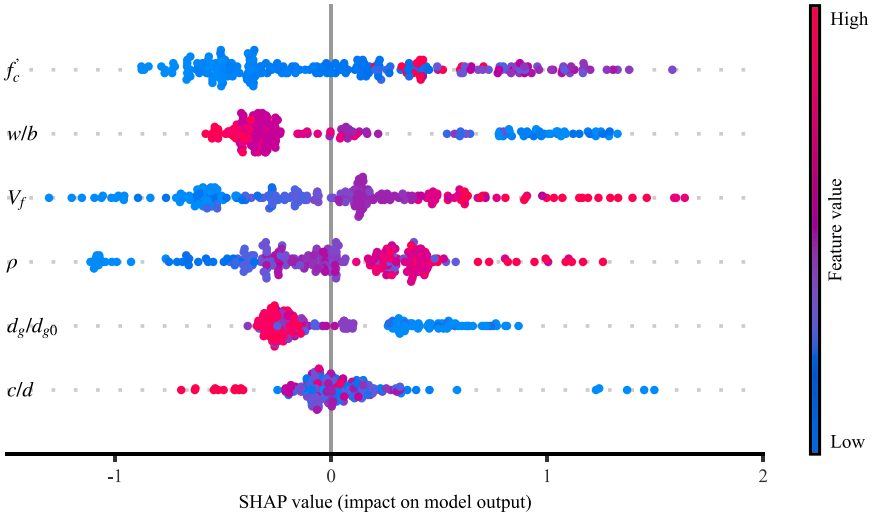

Fig. 9. SHAP summary plot (with feature selection).

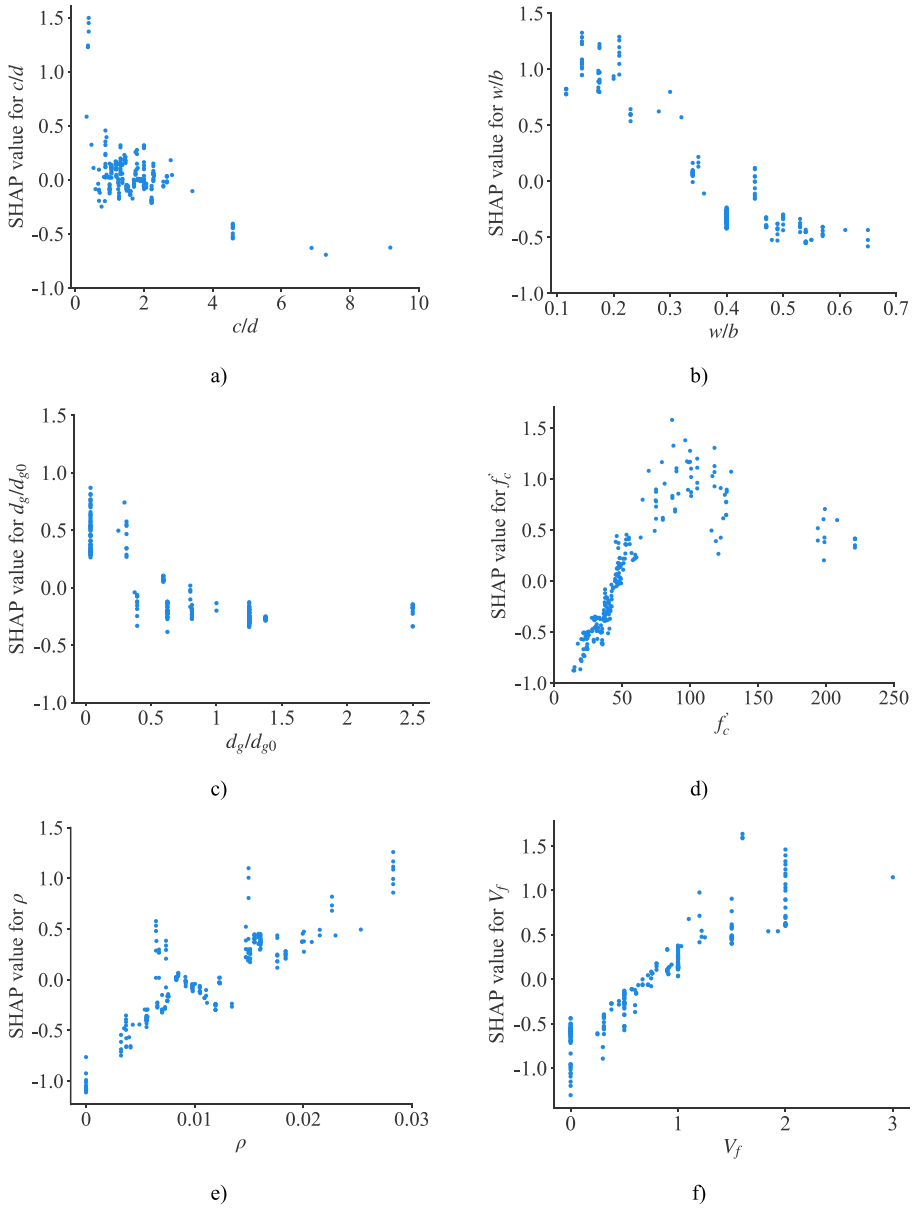

Fig. 10. Feature dependence plots of selected features and the target variable in the XGBoost model.

7.1. Effect of concrete compressive strength

When the concrete compressive strength $f_c^{'}$ is below about 75 MPa, an increase of concrete strength increases the punching shear strength v_p in the XGBoost model prediction. This agrees well with both the Narayanan and Darwish and Harajli *et al.* models. For the Higashiyama *et al.* model, the increase of PSS ends when the $f_c^{'}$ exceeds 50 MPa, which is due to the limitation of flexural strength of concrete. When the $f_c^{'}$ is over 75 MPa, the increase of concrete strength leads to gradual decrease of the punching shear strength. Although the trend is different with that of the mechanical models, similar trend can be found in Nguyen *et al.* [20] where a decrease of v_p can also be found when increasing the concrete strength only and keeping the fiber and reinforcement ratio the same. The decrease of v_p may be due to that the concrete become more brittle when the $f_c^{'}$ is higher than 75 MPa without changing the fiber volume. The XGBoost is able to consider this decrease, while the existing mechanical models may only consider the condition of FRC where $f_c^{'}$ is usually within 60 MPa and cannot detect the trend.

7.2. Effect of reinforcement ratio

The trend in the XGBoost model that higher punching shear strength v_p is achieved by increasing the reinforcement ratio ρcorresponds well with the two models presented in Fig. 11b. The Harajli *et al.* model does not consider the effect of ρ, so their results are always the same. Similar to the Narayanan and Darwish model, the XGBoost model considered the v_p when the $\rho = 0$, which is more important for HPFRC and UHPFRC slabs due to the higher contribution of the concrete matrix to the value v_p, as testified by Harris [52] and Park [53]. In addition, the XGBoost model indicated that very limited change when the ρ was over 1.5%. The limited increase of v_p due to high ρ has already been proven in FRC slabs in the research of Harajli *et al.* [15] and McHarg *et al.* [51]. Chanthabouala *et al.* [14] illustrated that the increase of ρ is limited in some cases, while it was significant in other cases in HPFRC slabs. However, this trend may need to be further confirmed by more experimental results on HPFRC and UHPFRC slabs with ρ of higher than 1.5%.

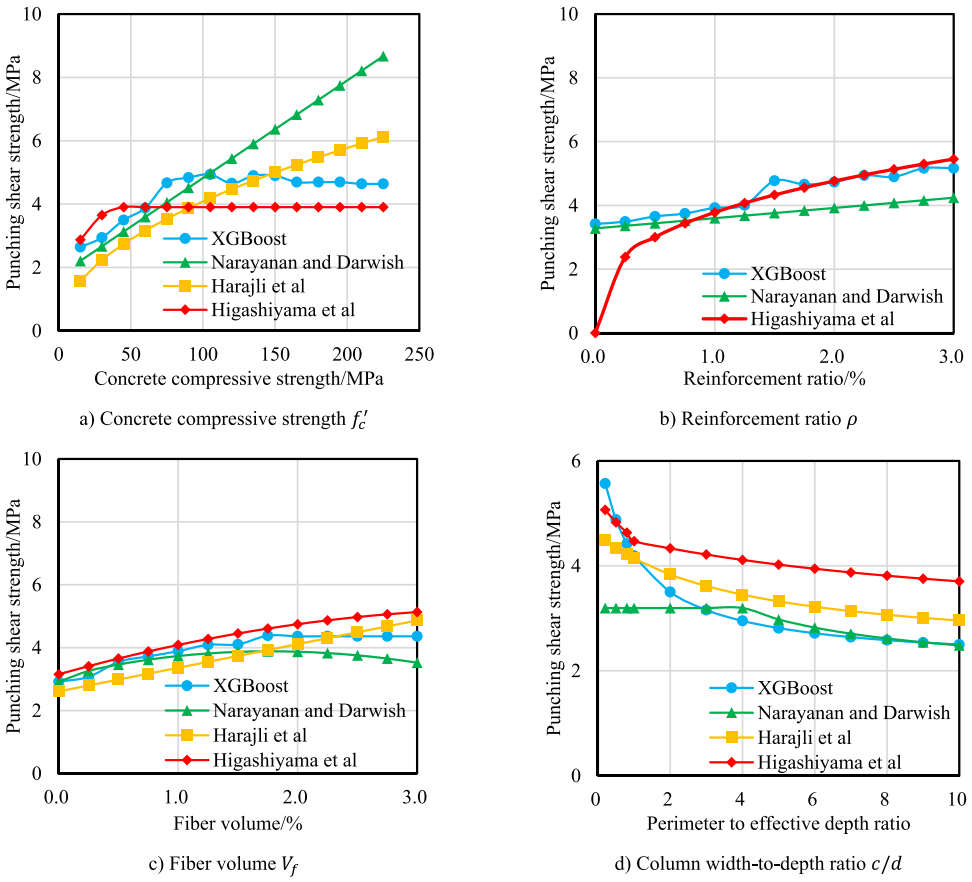

a) Concrete compressive strength f_c'

b) Reinforcement ratio ρ

c) Fiber volume V_f

d) Column width-to-depth ratio c/d

Fig. 11. Effects of four influential parameters on the punching shear strength of FRC slabs.

7.3. Effect of fiber volume

The punching shear strength v_p increases when the fiber volume V_f is below 2% in the XGBoost model, Harajli *et al.*, and Higashiyama *et al.* models, which agrees well with the existing test results [9,62,66]. In fact, the fiber volume has usually been the main investigated parameter in the research of FRC slabs. The Narayanan and Darwish model present an opposite trend of decreasing v_p when the fiber volume V_f reaches above 1.5%, which is due to the fact that the relation between the fiber factor F and flexural strength of concrete is based on the regression analysis of a limited number of FRC slabs [28]. When the V_f is above 2%, both the XGBoost model and Higashiyama *et al.* models indicated limited additional increase in v_p, which is mainly because there is only one specimen reported that has a fiber volume of 3% in Shoukry *et al.* [69], therefore, this trend should be investigated in future research.

7.4. Effect of column width-to-depth ratio

With the increase of the column width-to-depth ratio c/d, the punching shear strength v_p is gradually decreased in all the four models, which correlates well with the existing research on FRC and UHPFRC slabs [9,53,58]. This decrease is mainly due to the increased area of punching shear regions under the same depth of concrete slabs. Accordingly, progressive collapse becomes more likely after the initiation of critical shear cracks in the slabs. The decrease of v_p also stops in XGBoost model predictions when the ratio is above 4, which is due to the limited FRC slabs related to such cases [50].

In general, most of the trends of the four influential parameters in the proposed XGBoost model correlate well with the existing test results and the mechanical models. Some trends that do not conform to the mechanical models are either due to the limitations of the mechanical models, or the lack of pertinent data sets, which warrants the need for additional concerted research in the future. Nevertheless, the proposed XGBoost model has proved to be the most effective for predicting the punching shear strength of NSFRC, HPFRC and UHPFRC slabs in this study, which is promising for incorporation in generative design and for informing pertinent design code provisions.

8. Limitations and future directions

The proposed XGBoost model developed based on the newly established database can predict the punching shear strength of flat slabs for a wide range of FRC mixture compositions. It can also capture the influence of the various input parameters on the punching shear strength. Nevertheless, the accuracy and stability of the proposed XGBoost model may be affected by two limitations, thus future research directions ought to be pursued. First, in some conditions such as specimens made of UHPFRC, the number of data points is limited in the database and the value ranges of their parameters are also restricted. Experiments on HPFRC and UHPFRC flat slabs are needed in future research to improve the model performance. Apart from experimental test, finite element models validated by experimental data could also serve as an efficient method to enrich the database through numerical calculation. This can provide considerable additional data points and may help improve the performance of machine learning models through extended training and optimization. Second, the proposed models cannot derive explicit equations that would be user friendly and much easier for structural engineers to use in design practice. Accordingly, advanced ML tools such as deep learning algorithms, few-shot learning, and transfer learning can be considered to propose explicit, mechanism-related formulas to improve structural design and calculations [96]. Furthermore, the model proposed herein could be further applied to reliability assessment

and optimizations of the concrete structures [97,98].

9. Conclusions

An explainable machine learning model based on the XGBoost algorithm was developed in this study for predicting the punching shear strength of FRC flat slabs. The XGBoost model was trained through the procedure of data preprocessing, feature selection, hyperparameter tuning, and model validation on a newly developed comprehensive database, which includes 251 datasets measured on flat slabs made with NSFRC, HPFRC, and UHPFRC retrieved from the open literature. The performance of the proposed XGBoost model was appraised and compared to that of three other traditional ML models and six existing mechanical models. The effects of the six most significant features on the XGBoost model were quantitatively analyzed through SHAP analysis including a general feature effect summary and detailed feature dependence plots. Sensitivity analysis was also conducted on XGBoost model and three mechanical models for calculating punching shear strength of NSFRC slabs. Based on the results, the following conclusions are drawn:

1) The proposed XGBoost model achieved highest accuracy and lower variance in predicting the PSS of FRC slabs with MV value of 1.01, R^2 value of 0.99, MAE value of 0.17, and COV value of 0.07, which outperformed the other three ML models and six mechanical-based models.
2) Among the mechanical models, the Narayanan and Darwish model preformed the best, with MV value of 1.01, R^2 value of over 0.06, MAE value of less than 1.12 and COV value of 0.33. For the guarantee rates, the ACI 318–19 and Eurocode 2 models attained higher values in GR100, while ACI model yielded higher GR125 values.
3) Six features were identified as the most influential on the PSS of FRC slabs, among which compressive strength of concrete $f_c^{'}$, water-to-binder ratio w/b, steel fiber volume V_f, and longitudinal rebar ratio ρ were the four most influential. Although the w/b and $f_c^{'}$ are not entirely dependent, their simultaneous use better dissociates normal FRC from HSFRC and UHSFRC slabs.
4) The feature selection method was effective in removing redundant features without influencing the performance of the XGBoost model. The elimination of the five less influential features indicated that the shear span-to-depth ratio of the slabs and detailed fiber properties (other than the fiber volume) of the FRC may have little influence on the prediction performance.
5) SHAP analysis indicates that an increase of $f_c^{'}$, V_f, and ρ increases the PSS of FRC slabs, while an increase of c/d, w/b, and d_g/d_{g0} can decrease the PSS of FRC slabs. Both increasing and decreasing effects became less apparent above a certain threshold of the input parameters as follows ($f_c^{'}$=75 MPa, V_f=1.5%, c/d=4.5, w/b=0.4, d_g/d_{g0}=0.7, ρ=1.5%).
6) The trend of the four influential parameters ($f_c^{'}$, V_f, ρ, c/d) are also studied by sensitivity analysis of the XGBoost model, which obtained overall agreement with the mechanical models and can point out the necessity of further studies. The threshold of the four parameters were determined ($f_c^{'}$=75 MPa, V_f=2.0%, c/d=4, ρ=1.5%) and correlated well with the results in SHAP analysis.

To facilitate simplified use by material and structural engineers and stimulate concerted research among various research groups in the future, the present XGBoost model has been incorporated into an executable calculator, and the database including the test results and predictions of the proposed model have been listed. Both are available online at GitHub (https://github.com/MontrealCat/PSS-of-FRCs). With the proposed model and the associated calculator, structural engineers can quickly calculate the PSS with several easily accessed parameters and greatly facilitate the design and calculation of the structure.

CRediT authorship contribution statement

Liu Tongxu: Data curation, Formal analysis, Investigation, Methodology, Software, Visualization, Writing – original draft. **Cakiroglu Celal:** Data curation, Formal analysis, Investigation, Methodology, Validation, Visualization, Writing – original draft. **Wang Zhen:** Data curation, Investigation, Software, Validation, Visualization. **Nehdi Moncef L.:** Conceptualization, Project administration, Resources, Supervision, Writing – review & editing. **Islam Kamrul:** Data curation, Formal analysis, Investigation, Software, Validation, Visualization, Writing – original draft.

Declaration of Competing Interest

The authors declare that they have no known competing financial interests or personal relationships that could have appeared to influence the work reported in this paper.

Data Availability

Some or all data, models, or code generated or used during the study are available from the corresponding author upon request.

Acknowledgments

The first author gratefully acknowledge the financial support from the China Scholarship Council (CSC) during his PhD.

References

[1] Muttoni A. Punching shear strength of reinforced concrete slabs without transverse reinforcement. Acids Struct J 2008;105(4):440–50.
[2] Wu X, Yu S, Xue S, Kang THK, Hwang HJ. Punching shear strength of UHPFRC-RC composite flat plates. Eng Struct 2019;184:278–86.
[3] King S, Delatte N. Collapse of 2000 commonwealth avenue: Punching shear case study. J Perform Constr Facil 2004;18(1):54–61.
[4] Lawler N, Polak MA. Development of FRP shear bolts for punching shear retrofit of reinforced concrete slabs. J Compos Constr 2011;15(4):591–601.
[5] Yankelevsky DZ, Karinski YS, Brodsky A, Feldgun VR. Evaluation of punching shear design criteria to prevent progressive collapse of RC flat slabs. Int J Prot Struct 2021;12(2):174–205.
[6] Maya L, Ruiz MF, Muttoni A, Foster S. Punching shear strength of steel fibre reinforced concrete slabs. Eng Struct 2012;40:83–94.
[7] Fernández RM, Mirzaei Y, Muttoni A. Post-punching behavior of flat slabs. Acids Struct J 2013;110(5):801–12.
[8] Michels J, Waldmann D, Maas S, Zürbes A. Steel fibers as only reinforcement for flat slab construction–Experimental investigation and design. Constr Build Mater 2012;26(1):145–55.
[9] Nguyen-Minh L, Rovňák M, Tran-Quoc T, Nguyenkim K. Punching shear resistance of steel fiber reinforced concrete flat slabs. Procedia Eng 2011;14:1830–7.
[10] Tan KH, Venkateshwaran A. Punching shear in steel fiber-reinforced concrete slabs with or without traditional reinforcement. Acids Struct J 2019;116(3):107–18.
[11] Theodorakopoulos D, Swamy N. Contribution of steel fibers to the strength characteristics of lightweight concrete slab-column connections failing in punching shear. Acids Struct J 1993;90(4):342–55.
[12] Shaaban A, Gesund H. Punching shear strength of steel fiber reinforced concrete flat plates. Acids Struct J 1994;91(4):406–14.
[13] Swamy RN, Ali SAR. Punching shear behavior of reinforced slab-column connections made with steel fiber concrete. Am Concr Inst Proc 1982;79:392–406.
[14] Chanthabouala K, Teng S, Chandra J, Tan KH, Ostertag CP. Punching Tests of Double-Hooked-End Fiber-Reinforced Concrete Slabs. Acids Struct J 2018;115(6):1777–89.
[15] Harajli MH, Maalouf D, Khatib H. Effect of fibers on the punching shear strength of slab-column connections. Cem Concr Compos 1995;17(2):161–70.
[16] Choi KK, Taha MMR, Park HG, Maji AK. Punching shear strength of interior concrete slab–column connections reinforced with steel fibers. Cem Concr Compos 2007;29(5):409–20.
[17] Cheng MY, Parra-Montesinos GJ. Evaluation of steel fiber reinforcement for punching shear resistance in slab-column connections–Part I: monotonically increased load. Acids Struct J 2010;107(1):101–9.
[18] Naaman AE. Engineered steel fibers with optimal properties for reinforcement of cement composites. J Adv Concr. Tech 2003;1(3):241–52.

[19] Sousa AM, Lantsoght EO, Genikomsou AS, Krahl PA, Mounir K. Behavior and punching capacity of flat slabs with the rational use of UHPFRC: NLFEA and analytical predictions. Eng Struct 2021;244:112774.
[20] Nguyen TN, Nguyen TT, Pansuk W. Experimental study of the punching shear behavior of high performance steel fiber reinforced concrete slabs considering casting directions. Eng Struct 2017;131:564–73.
[21] Sarsam KF, Hassan HF. Punching shear failure characteristics of flat slabs using reactive and modified powder concrete with steel fibers. J Eng Sustain Dev 2013; 17(5):124–40.
[22] Joh CB, Kim BS, Hwang HH, Choi KK, Choi SH. Punching shear strength of deck slabs made of ultra high performance concrete. J Korea Inst Struct Maint Insp 2011;15(4):221–31.
[23] ACI (American Concrete Institute). Building Code Requirements for Structural Concrete and Commentary on Building Code Requirements for Structural Concrete. Farmington Hills, MI: ACI,; 2019. p. 318–9.
[24] BS 8110. Structural use of concrete, Part 1: Code of practice for design and construction. British Standards Institute; 1997.
[25] EN 1992–1-1. Eurocode 2: Design of concrete structures – Part 1–1:General rules and rules for building. 2004.
[26] Abbood IA, Al-Bayati AF. Punching shear strength of steel fibre reinforced concrete flat slabs: a literature review and design codes evaluation. IOP Conf Ser: Mater Sci Eng 2021;1067(1):012061.
[27] Higashiyama H, Ota A, Mizukoshi M. Design equation for punching shear capacity of SFRC slabs. Int J Concr Struct Mater 2011;5(1):35–42.
[28] Narayanan R, Darwish I. Punching shear tests on steel-fibre-reinforced micro-concrete slabs. Maga Concr Res 1987;39(138):42–50.
[29] Kueres D, Polak MA, Hegger J. Two-parameter kinematic theory for punching shear in steel fiber reinforced concrete slabs. Eng Struct 2020;205:110086.
[30] Li H, Li L, Li L, Zhou J, Mu R, Xu M. Influence of fiber orientation on the microstructures of interfacial transition zones and pull-out behavior of steel fiber in cementitious composites. Cem Concr Compos 2022;128:104459.
[31] Neto BNM, Barros JA, Melo GS. A model for the prediction of the punching resistance of steel fibre reinforced concrete slabs centrically loaded. Constr Build Mater 2013;46:211–23.
[32] Abdallah S, Fan M, Zhou X. Pull-out behaviour of hooked end steel fibres embedded in ultra-high performance mortar with various W/B ratios. Int J Concr Struct Mater 2017;11(2):301–13.
[33] Wille K, Naaman AE. Pullout behavior of high-strength steel fibers embedded in ultra-high-performance concrete. Acids Mater J 2012;109(4):479–88.
[34] Xie Y, Sichani ME, Padgett JE, DesRoches R. The promise of implementing machine learning in earthquake engineering: a state-of-the-art review. Earthq Spectra 2020; 36(4):1769–801.
[35] Asteris PG, Nozhati S, Nikoo M, Cavaleri L, Nikoo M. Krill herd algorithm-based neural network in structural seismic reliability evaluation. Mech Adv Mater Struct 2019;26(13):1146–53.
[36] Chaabene WB, Flah M, Nehdi ML. Machine learning prediction of mechanical properties of concrete: Critical review. Constr Build Mater 2020;260:119889.
[37] Li Z, Yoon J, Zhang R, Rajabipour F, Srubar WV, Dabo I, et al. Machine learning in concrete science: applications, challenges, and best practices. npj Comput Mater 2022;8(1):1–17.
[38] Nguyen H, Vu T, Vo TP, Thai HT. Efficient machine learning models for prediction of concrete strengths. Constr Build Mater 2021;266:120950.
[39] Feng DC, Liu ZT, Wang XD, Chen Y, Chang JQ, Wei DF, et al. Machine learning-based compressive strength prediction for concrete: An adaptive boosting approach. Constr Build Mater 2020;230:117000.
[40] Rahman J, Ahmed KS, Khan NI, Islam K, Mangalathu S. Data-driven shear strength prediction of steel fiber reinforced concrete beams using machine learning approach. Eng Struct 2021;233:111743.
[41] Liu T, Wang Z, Zeng J, Wang J. Machine-learning-based models to predict shear transfer strength of concrete joints. Eng Stuct 2021;249:113253.
[42] Asteris PG, Armaghani DJ, Hatzigeorgiou GD, Karayannis CG, Pilakoutas K. Predicting the shear strength of reinforced concrete beams using artificial neural networks. Comput Concr Int J 2019;24(5):469–88.
[43] Faridmehr I, Nehdi M, Baghban MH. Novel informational bat-ANN model for predicting punching shear of RC flat slabs without shear reinforcement. Eng Struct 2022;256:114030.
[44] Wu Y, Zhou Y. Prediction and feature analysis of punching shear strength of two-way reinforced concrete slabs using optimized machine learning algorithm and Shapley additive explanations. Mech Adv Mater Struct 2022:1–11.
[45] Mangalathu S, Shin H, Choi E, Jeon JS. Explainable machine learning models for punching shear strength estimation of flat slabs without transverse reinforcement. J Build Eng 2021;39:102300.
[46] Nguyen HD, Truong GT, Shin M. Development of extreme gradient boosting model for prediction of punching shear resistance of r/c interior slabs. Eng Struct 2021; 235:112067.
[47] Truong GT, Hwang HJ, Kim CS. Assessment of punching shear strength of FRP-RC slab-column connections using machine learning algorithms. Eng Struct 2022;255: 113898.
[48] Vu DT, Hoang ND. Punching shear capacity estimation of FRP-reinforced concrete slabs using a hybrid machine learning approach. Struct Infrastruct Eng 2016;12(9): 1153–61.
[49] Hoang ND. Estimating punching shear capacity of steel fibre reinforced concrete slabs using sequential piecewise multiple linear regression and artificial neural network. Measurement 2019;137:58–70.
[50] Lu S, Koopialipoor M, Asteris PG, Bahri M, Armaghani DJ. A novel feature selection approach based on tree models for evaluating the punching shear capacity of steel fiber-reinforced concrete flat slabs. Materials 2020;13(17):3902.
[51] Alotaib E, Mostafa IO, Nassif N, Omar M, Arab MG. Prediction of punching shear capacity for fiber-reinforced concrete slabs using neuro-nomographs constructed by machine learning. J Struct Eng 2021;147(6):04021075.
[52] Feng DC, Wang WJ, Mangalathu S, Taciroglu E. Interpretable XGBoost-SHAP machine-learning model for shear strength prediction of squat RC walls. J Struct Eng 2021;147(11):04021173.
[53] Li QF, Song ZM. High-performance concrete strength prediction based on ensemble learning. Constr Build Mater 2022;324:126694.
[54] Chen T, He T, Benesty M, Khotilovich V, Tang Y, Cho H, et al. Xgboost: extreme gradient boosting. R Package Version 2015;1(4):1–4.
[55] Cortes C, Vapnik V. Support-vector networks. Mach Learn 1995;20(3):273–97.
[56] Liu T, Wang Z, Long Z, Zeng J, Wang J, Zhang J. Direct shear strength prediction for precast concrete joints using the machine learning method. J Bridge Eng 2022; 27(5):04022026.
[57] Wang Z, Liu T, Long Z, Wang J, Zhang J. A machine-learning-based model for predicting the effective stiffness of precast concrete columns. Eng Struct 2022;260: 114224.
[58] Peterson LE. K-nearest neighbor. Scholarpedia 2009;4(2):1883.
[59] Akbari M, Deligani VJ. Data driven models for compressive strength prediction of concrete at high temperatures. Front Struct Civ Eng 2020;14(2):311–21.
[60] Liang M, Chang Z, Wan Z, Gan Y, Schlangen E, Šavija B. Interpretable Ensemble-Machine-Learning models for predicting creep behavior of concrete. Cem Concr Compos 2022;125:104295.
[61] Biau G, Scornet E. A random forest guided tour. Test 2016;25(2):197–227.
[62] Tan KH, Paramasivam P. Punching shear strength of steel fiber reinforced concrete slabs. J Mater Civ Eng 1994;6(2):240–53.
[63] McHarg PJ, Cook WD D, Mitchell, Yoon YS. Benefits of concentrated slab reinforcement and steel fibers on performance of slab-column connections. Acids Struct J 2000;97(2):225–34.
[64] Harris DK. Characterization of Punching Shear Capacity of Thin UHPC Plates. Doctoral dissertation. USA: Virginia Tech; 2004.
[65] Park JH, Hong SG. Estimation of Punching Shear Strength for Ultra High Performance Concrete Thin Slab. J Korean Assoc Spat Struct 2015;15(2):95–103.
[66] Ozden S, Ersoy U, Ozturan T. Punching shear tests of normal-and high-strength concrete flat plates. Can J Civ Eng 2006;33(11):1389–400.
[67] Yaseen AA. Punching Shear Strength of Steel Fiber High Strength Reinforced Concrete Slabs. Iraq: University of Salahaddin-Erbil; 2006.
[68] Naaman AE, Likhitruangsilp V, Parra-Montesinos G. Punching shear response of high-performance fiber-reinforced cementitious composite slabs. Acids Mater J 2007;104(2):170.
[69] Hanai JB, Holanda KMA. Similarities between punching and shear strength of steel fiber reinforced concrete (SFRC) slabs and beams. Ibracon Struct Mater J 2008;1 (1):1–16.
[70] Joh C, Hwang H, Kim B. Punching shear and flexural strengths of ultra high performance concrete slabs. High Perform Struct Mater IV 2008:97–106.
[71] Wang XW, Tian WL, Huang ZY, Zhou MJ, Zhao XY. Analysis on punching shear behavior of the raft slab reinforced with steel fibers. Key Eng Mater 2009;400: 335–40.
[72] Yang JM, Yoon YS, Cook WD, Mitchell D. Punching shear behavior of two-way slabs reinforced with high-strength steel. Acids Struct J 2010;107(4):468–75.
[73] Hassan FH. Punching Shear Behavior of Normal and Modified Reactive Powder Concretes Slabs (PhD Thesis). Baghdad, Iraq: Al-Mustansiriya University; 2012.
[74] Grimaldi A, Meda A, Rinaldi Z. Experimental behaviour of fibre reinforced concrete bridge decks subjected to punching shear. Compos Part B: Eng 2013;45(1):811–20.
[75] Al-Quraishi HAA. Punching Shear Behavior of UHPC Flat Slabs (PhD Thesis). Kassel, German: University of Kassel; 2014.
[76] Caratelli A, Imperatore S, Meda A, Rinaldi Z. Punching shear behavior of lightweight fiber reinforced concrete slabs. Compos Part B: Eng 2016;99:257–65.
[77] Gouveia ND, Lapi M, Orlando M, Faria DM, Ramos AMP. Experimental and theoretical evaluation of punching strength of steel fiber reinforced concrete slabs. Struct Concr 2018;19(1):217–29.
[78] Abdel-Rahman AM, Hassan NZ, Soliman AM. Punching shear behavior of reinforced concrete slabs using steel fibers in the mix. HBRC J 2018;14(3):272–81.
[79] Landler J., Fischer O. Punching shear capacity of steel fiber reinforced concrete slab-column connections, In Proceedings IABSE Congress 2019.
[80] Kadhum MM, Harbi SM, Khamees SS, Abdulraheem MS, Farsangi EN. Punching shear behavior of flat slabs utilizing reactive powder concrete with and without flexural reinforcement. Pract Period Struct Des Constr 2021;26(1):04020060.
[81] Shoukry ME, Tarabia AM, Yassin AM. Punching shear strength of ultra-high-performance fibre concrete slab–column connections. Proc Inst Civ Eng-Struct Build 2021;14:1–13.
[82] Choi K, Taha MMR, Sherif AG. Simplified punching shear design method for slab-column connections using fuzzy learning. Acids Struct J 2007;104(4):438–47.
[83] Mashrei MA, Mahdi AM. An adaptive neuro-fuzzy inference model to predict punching shear strength of flat concrete slabs. Appl Sci 2019;9(4):809.
[84] Sarir P, Chen J, Asteris PG, Armaghani DJ, Tahir MM. Developing GEP tree-based, neuro-swarm, and whale optimization models for evaluation of bearing capacity of concrete-filled steel tube columns. Eng Comput 2021;37:1–19.
[85] Wakjira TG, Al-Hamrani A, Ebead U, Alnahhal W. Shear capacity prediction of FRP-RC beams using single and ensenble explainable machine learning models. Compos Struct 2022;287:115381.
[86] Pedregosa F, Varoquaux G, Gramfort A, Michel V, Thirion B, Grisel O, et al. Scikit-learn: machine learning in python. J Mach Learn Res 2011;12:2825–30.

[87] Zhang J, Zhang M, Dong B, Ma H. Quantitative evaluation of steel corrosion induced deterioration in rubber concrete by integrating ultrasonic testing, machine learning and mesoscale simulation. Cem Concr Compos 2022;128:104426.
[88] Nassif N, Al-Sadoon ZA, Hamad K, Altoubat S. Cost-based optimization of shear capacity in fiber reinforced concrete beams using machine learning. Struct Eng Mech 2022;83(5):671.
[89] Santos J, Henriques AA. Span-to-depth ratio limits for RC continuous beams and slabs based on MC2010 and EC2 ductility and deflection requirements. Eng Struct 2021;228:111565.
[90] Lundberg SM, Lee S-I. A unified approach to interpreting model predictions. Proceedings of the 31st Conference on Neural Information Processing Systems (NIPS 2017). CA, USA: Long Beach,; 2017. p. 4–9.
[91] Ye B, Zhang Y, Han J, Pan P. Effect of water to binder ratio and sand to binder ratio on shrinkage and mechanical properties of high-strength engineered cementitious composite. Constr Build Mater 2019;226:899–909.
[92] Arora A, Almujaddidi A, Kianmofrad F, Mobasher B, Neithalath N. Material design of economical ultra-high performance concrete (UHPC) and evaluation of their properties. Cem Concr Compos 2019;104:103346.
[93] Trejo D, Reinschmidt K. Justifying materials selection for reinforced concrete structures. I: Sensitivity analysis. J Bridge Eng 2007;12(1):31–7.
[94] Mostafa, O., Alotaibi, E., Al-Ateyat, A., Nassif, N., Barakat, S. Prediction of Punching Shear Capacity for Fiber-Reinforced Polymer Concrete Slabs Using Machine Learning. In 2022 Advances in Science and Engineering Technology International Conferences (ASET) IEEE 2022:1–6.
[95] Al-Sadoon ZA, Alotaibi E, Omar M, Arab MG, Tahmaz A. AI-driven prediction of tunneling squeezing: comparing rock classification systems. Geotech Geol Eng 2023;2023:1–23.
[96] Pak H, Paal SG. Evaluation of transfer learning models for predicting the lateral strength of reinforced concrete columns. Eng Struct 2022;266:114579.
[97] Alotaibi E, Nassif N, Barakat S. Data-driven reliability and cost-based design optimization of steel fiber reinforced concrete suspended slabs. Struct Concr 2023; 24:1856–67.
[98] Nassif N, Al-Sadoon ZA, Hamad K, Altoubat S. Cost-based optimization of shear capacity in fiber reinforced concrete beams using machine learning. Struct Eng Mech 2022;83(5):671.